Two-proton radioactivity and three-body decay. II. Exploratory studies of lifetimes and correlations

L. V. Grigorenko[1,2] and M. V. Zhukov[3]
[1]*Gesellschaft für Schwerionenforschung mbH, Planckstrasse 1, D-64291 Darmstadt, Germany*
[2]*Russian Research Center "The Kurchatov Institute," RU-123182 Moscow, Russia*
[3]*Department of Physics, Chalmers University of Technology and Göteborg University, S-41296 Göteborg, Sweden*
(Received 15 August 2003; published 26 November 2003)

Theoretical studies of prospective $2p$ emitters are performed in a three-body core$+p+p$ model. Lifetime dependencies on the decay energy are calculated for ^{45}Fe, ^{48}Ni, ^{54}Zn, ^{58}Ge, ^{62}Se, ^{66}Kr, and compared to the quasiclassical estimates. The observation of products from the in-flight decays is discussed as an important technique supplementing a standard implantation method for a broad range of lifetimes of prospective two-proton emitters. The sensitivity of the model to various aspects of nuclear dynamics is demonstrated on the ^{45}Fe example. Possible momentum correlations for emitted protons are discussed with the emphasis on ^{19}Mg and ^{45}Fe. We study convergence and stability of theoretical momentum distributions with respect to different physical and numerical aspects of the model. Opportunities to extract valuable information on $2p$ emission from incomplete kinematics decay data are discussed.

DOI: 10.1103/PhysRevC.68.054005 PACS number(s): 21.45.+v, 21.60.Gx, 21.10.Tg, 23.50.+z

I. INTRODUCTION

Recently a quantum mechanical method has been developed, which allows a study of the two-proton (three-body) decay phenomenon in a three-body cluster model [1,2]. Within the method the lifetime dependencies on the decay energy and correlations among the decay fragments can be obtained. For light systems (say, up to ^{19}Mg) the Coulomb displacement energies can be reliably calculated. The method has been applied to a range of nuclear systems (^{12}O, ^{16}Ne [3], ^{6}Be, ^{8}Li*, ^{9}Be* [4], ^{17}Ne, ^{19}Mg [5], ^{30}Ar, ^{34}Ca, ^{45}Fe [6]) providing sometimes intriguing results.

The idea of two-proton emission studies came out more than 40 years ago [7]. Possible modes of the two-proton (three-body) decay are discussed in details in Ref. [2]. We concentrate on "true" two-proton emission, which, in terms of Ref. [7], means that the decay by emission of one proton and subsequently the other (sequential decay) is impossible due to separation energy conditions, and both protons should be emitted simultaneously. This is a pure quantum mechanical phenomenon which has no classical analog. It was clear from the very beginning [7] that two-proton radioactivity should have different lifetime systematics compared to ordinary binary decays and specific correlations among decay products. However, for a long time theoretical studies of the phenomenon have been carried out mostly in the framework of quasiclassical models [8–12], having a limited predictive power. Being clearly an approximation to the quantum mechanical results, the quasiclassical models still remain methodologically important. It was demonstrated in Ref. [6] under which conditions the results of quasiclassical models become compatible with the three-body model results, thus providing a shortcut for bulky three-body calculations. There are, nevertheless, observables for which quasiclassics cannot provide any information. Realistic momentum distributions of decay products cannot be obtained in quasiclassical approaches due to the evident reason of absence of the dynamics in these models.

The theoretical developments [1–6] coincided in time with the revival of the experimental interest to studies of the two-proton radioactivity based on modern advances in radioactive nuclear beam techniques (see also reviews of earlier activities in Refs. [2,13]). For example, very promising results have recently been obtained for the decay of the ^{45}Fe ground state [14,15]. Experiments are being planned to study decays of ^{19}Mg, ^{48}Ni, ^{54}Zn, and to improve the results for ^{45}Fe. Decent theoretical estimates are important for planning experiments in the field because a minor uncertainty in the two-proton separation energy can easily lead to a significant change of the lifetime, which may require a different experimental approach [5,6].

The most conventional experimental approach to study the lifetime is to implant the nucleus and to wait for its decay. For lifetimes of the $2p$ emission longer than 10^{-3}–10^{-1} s, the observation of the $2p$ decay should be suppressed by the β decay (electron capture). For $2p$ lifetimes shorter than hundreds of nanoseconds the implantation is impossible as the nuclei decay before they can be implanted. It was suggested in Refs. [5,16] to use the "decay-in-flight" technique for the lifetime range from $5-10$ ps to $10-100$ ns. For this lifetime range the flight path of a nucleus before decay is macroscopic (from millimeters to meters for a relativistic primary beam). The reconstruction of fragment trajectories allows to recover the density of the decay vertexes along the trajectory and hence to deduce the lifetime. For lifetimes shorter than a few picoseconds the decay occurs directly in the target and no lifetime derivation is possible. Only when the width achieves some tens of kiloelectron-volt, it can be defined using the invariant (missing) mass method. Thus, there is a nine orders of magnitude gap on the lifetime scale, not accessible by the existing experimental techniques, while the regions where the $2p$ lifetimes are measurable are represented by quite narrow bands.

This paper has several important tasks.

(i) First of all we wanted more or less to complete a simple survey of the 2*p* decay candidates with $Z<40$. We have performed exploratory studies of ^{54}Zn, ^{58}Ge, ^{62}Se, ^{66}Kr, and completed them for ^{48}Ni along the systematic guidelines defined in Ref. [6].

(ii) In this paper for the first time we provide a detailed discussion of procedure for derivation of momentum correlations among the decay products and study carefully stability of these calculations. The corresponding experimental complete decay information is beginning to emerge in the literature, although yet only for the neutron dripline [17].

(iii) We pay special attention to ^{19}Mg and ^{45}Fe nuclei. In the previous studies [5,6] we concentrated on the lifetime issues. Here we are interested in the connection between lifetimes, structure, and correlations. The ^{19}Mg and ^{45}Fe are the most likely new 2*p* emitters for which the correlations have a chance to be measured in the observable future.

(iv) We demonstrate that valuable information, allowing to distinguish different theoretical models, can be obtained from incomplete information about correlations (projected distributions). Such projected distributions can be measured by the in-flight decay technique, which supplements a standard implantation method for a broad range of lifetimes of prospective two-proton emitters.

(v) In the end of the paper we provide overall discussion, including the review of our previous work [1–6] on 2*p* emission. We also summarize our current understanding of prospectives of experimental studies of 2*p* decays.

The unit system $\hbar=c=1$ is used in the article.

II. EXPLORATORY STUDIES OF PROSPECTIVE 2P EMITTERS: ^{48}NI,^{54}ZN,^{58}GE,^{62}SE,^{66}KR

Theoretical lifetime calculations for particle emitters consist roughly of two ingredients: determination of the decay energy and determination of the lifetime at given decay energy. The decay energy can be known from experiment, but there are many exotic nuclei for which this value is not available. The three-body model we use can provide a good structure description (and thus give reliable separation energies) only for the lightest systems. For heavier ones we have to rely on other theoretical calculations and systematics studies.

A determination of the lifetime at given decay energy in our model has methodologically much in common with the *R* matrix phenomenology as it is applied to ordinary two-body decays. In Refs. [2,6] we described what we call a "systematic l^2" model of the two-proton decay. In this model we take a realistic *p*-*p* interaction, but the width of the core-*p* interaction is taken from systematics and the depth is fitted so that the lowest state in this potential corresponds to the known (extrapolated) separation energy in the core-*p* subsystem. Varying components of the core-*p* interaction for different *l* values it is possible to vary the internal structure of the 2*p* emitter. We characterize the internal structure of the wave function (WF) by the probabilities of the l^2 configuration

$$W(l)=\int_0^{\rho_{int}} d\rho\ \rho^5 \int d\Omega_\rho d\Omega_\kappa \Psi_3^{(+)\dagger}\hat{P}_{l_x=l}\hat{P}_{l_y=l}\Psi_3^{(+)}.$$

Detailed definitions of ingredients can be found in Sec. IV; $\hat{P}_i$ are projectors on the states with definite angular momenta associated with Jacobi vectors *X* and *Y*, ρ_{int} should be taken about 20 fm. Calculated in "Y" Jacobi system these values closely correspond to shell-model probabilities of l^2 configurations for valence protons because for nuclear systems with heavy core the Jacobi vectors *X* and *Y* (in Y Jacobi system) closely correspond to shell-model single-particle coordinates calculated from the abstract center.

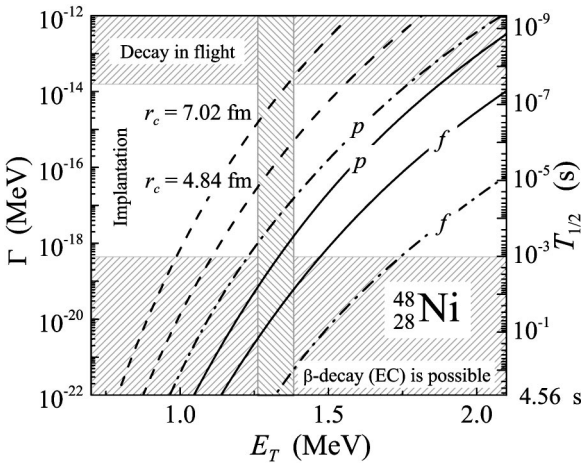

FIG. 1. The ^{48}Ni lifetime as a function of the 2*p* decay energy. The solid curves correspond to the three-body calculations with different dominating l^2 components [2,6]. The dashed curves correspond to the diproton estimates with different channel radii. The dash-dotted curves correspond to the simultaneous emission estimates for different *l* values. In this and in the following lifetime plots the horizontal hatched bands correspond to different types of possible experiments (see Ref. [5]) and vertical bands correspond to expected decay energies (see compilation in Table II).

The two-proton separation energy is adjusted using a short-range three-body force which is not large in the barrier region and hence does not influence the penetration process. The model formulated in this way allows to work with poorly studied systems as it does not require much input. The model does not pretend to provide a realistic internal structure for the studied nuclei, but has enough freedom to simulate it and thus to study the effects of various dynamics. In the asymptotic region the model employs approximate boundary conditions of the three-body Coulomb problem [2] and it gives an opportunity to calculate consistently the penetration process.

The lifetime dependencies on the decay energy calculated in the three-body l^2, diproton, and simultaneous emission models (see Ref. [6] for more details) are given in Figs. 1–5. The relation between width in million electron volt and lifetime $T_{1/2}$ in seconds is given by

$$\Gamma = 4.56\times 10^{-22}(\mathrm{MeVs})/T_{1/2}.$$

For some of these nuclei we can expect a strong p/f configuration mixing. The curves calculated in the assumption about total domination of one of the configurations (p^2 of f^2) form for each nucleus a corridor in which the real lifetime curve should then reside. The simultaneous emission model is also forming a corridor, but this corri-

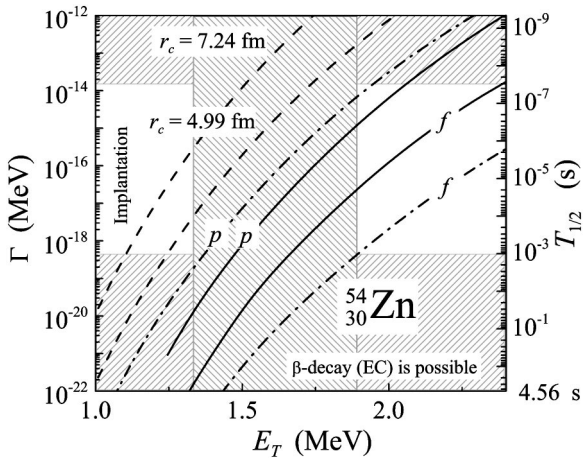

FIG. 2. The ^{54}Zn lifetime as a function of the 2p decay energy (see the caption of Fig. 1 for details).

dor is much broader than that obtained in the three-body calculations. Finally, the diproton model is providing the upper limit for the width, as shrinking of the three-body phase space to the two-body one should lead to an overestimation of the width. So, we have a sequence of models of an increasing sophistication, which presents (as we hope) a closer and closer approximation to the real situation.

We expect that ^{45}Fe and ^{66}Kr are characterized by a significant p/f mixing (probably with the f^2 configuration prevailing), in ^{48}Ni the f^2 is dominating, in ^{54}Zn, ^{58}Ge, and ^{62}Se the p^2 is dominating. The decay of nuclei with the dominating f^2 configuration is dynamically the most complicated (and thus having the largest theoretical uncertainties) process. It suggests first of all subbarrier transitions to the lower-l configurations (p^2 or/and s^2), and only after that tunneling through the Coulomb barrier takes place.

In Figs. 1–5 the horizontal hatched areas represent lifetime regions, where different experimental techniques are required to study the 2p decays. The vertical hatched bands show the possible decay energy according to calculations and systematics (see compilation in Table II). General overview of prospective 2p emitters is provided in Sec. V.

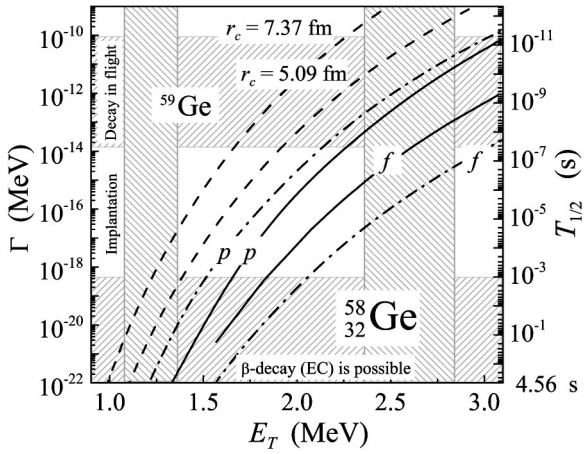

FIG. 3. The ^{58}Ge lifetime as a function of the 2p decay energy (see the caption of Fig. 1 for details).

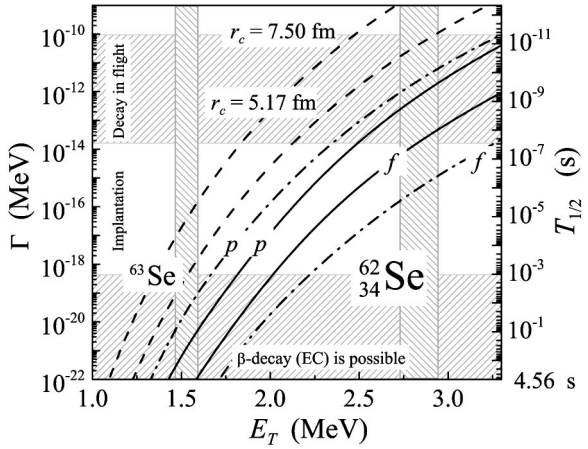

FIG. 4. The ^{62}Se lifetime as a function of the 2p decay energy (see the caption of Fig. 1 for details).

III. SENSITIVITY TO THE MODEL ASSUMPTIONS ON EXAMPLE OF ^{45}Fe

The largest uncertainty in the lifetime calculations is connected with uncertainty of the 2p decay energy. A variation of the decay energy at the level of 100 keV leads to 1–2 orders of magnitude variation in the lifetime. As we have seen above, the next important source of the uncertainty is the internal structure of the decaying system, which we consider in our model in an approximate way. It is important to understand the sensitivity of the calculations to this and some other aspect of the model. Below we provide the required illustration on the example of ^{45}Fe, where the 2p radioactivity have already been observed. This is useful for several reasons: (i) the ^{45}Fe is an important candidate for further (and more detailed) studies and (ii) the combination of factors (for example, the presumably non-negligible p/f mixing) make this nucleus the least "predictable" of all those we have studied.

In Fig. 6 the results of calculations [6] for the three-body and simultaneous emission models are given for ^{45}Fe in a larger scale. The circle and square show the experimental

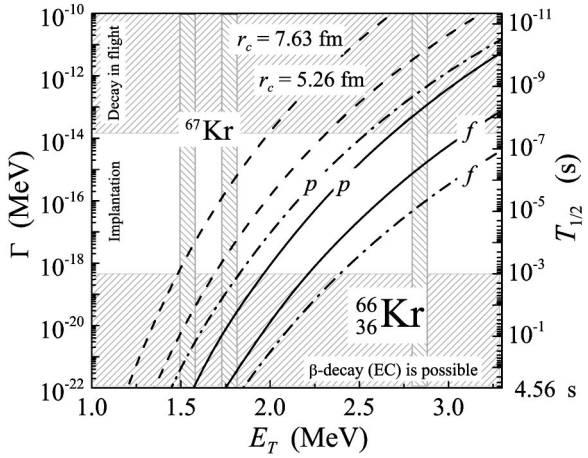

FIG. 5. The ^{66}Kr lifetime as a function of the 2p decay energy (see the caption of Fig. 1 for details).

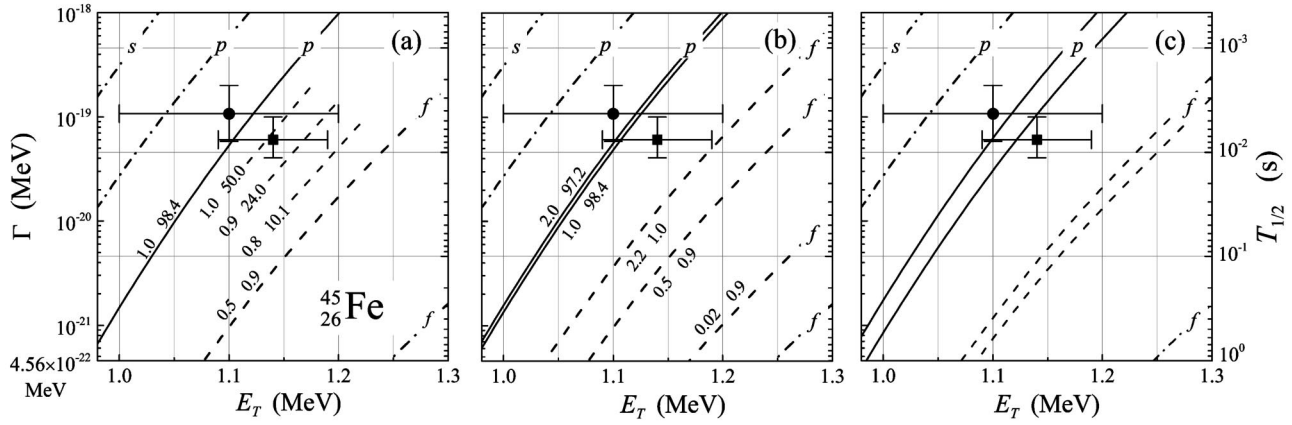

FIG. 6. The lifetime of ^{45}Fe as a function of the $2p$ decay energy in the framework of l^2 three-body model. Sensitivity of the results to different aspects of the model. The numerical labels on the curves show the weights of the s^2 and p^2 configurations in percent; the weight of d^2 is ordinarily negligible in these calculations, so the rest of the structure is f^2 configuration. The solid curves are for calculations with p^2 dominating. The dashed curves are for cases of p/f mixing or f^2 domination. The dash-dotted curves are simultaneous emission estimates as they are given in Ref. [6].

results from Ref. [14] [E_T=1100(100)keV,$T_{1/2}=3.2^{+2.6}_{-1.0}$ ms] and Ref. [15] [E_T=1140(50)keV,$T_{1/2}=5.7^{+2.7}_{-1.4}$ ms], respectively. In this figure the experimental data are corrected for expected (not yet measured!) 25% β-decay branch of ^{45}Fe with the corresponding uncertainty included in the upper width error bar. In panel (a) we demonstrate the dependence of the width on the p/f ratio. As it will be discussed below (see Fig. 10) this ratio influences the correlations among decay products. In panel (b) we show the sensitivity of the width to the variation of the s^2 configuration. While in the case of a pure p^2 structure of ^{45}Fe there is practically no sensitivity, the width in the case of a pure f^2 configuration is influenced strongly by the s^2 admixture.

One can see that within the current uncertainty of experimental data the three-body decay calculations are consistent with a broad range of possible ^{45}Fe structures, excluding only the extreme case of the f^2 configuration domination. The width curves corresponding to the realistic shell-model structure of ^{45}Fe (1–2% of s^2 and 10–15% of p^2 [18]) are currently passing closer to the lower error bar. It is, however, too early to draw definite conclusions from this fact for both theoretical (for example, the unknown exactly p/f ratio) and experimental (for example, the unknown β-decay branching) reasons.

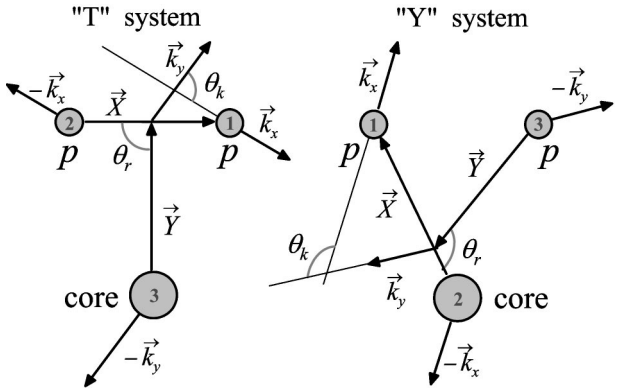

FIG. 7. Jacobi vectors for three particles in coordinate and in momentum spaces in T and Y Jacobi systems. It should be understood that planes defined by pairs $\{\mathbf{X},\mathbf{Y}\}$ and $\{\mathbf{k}_x,\mathbf{k}_y\}$ do not coincide in a general case.

In panel (c) we show the sensitivity of the lifetime to the variation of the core-p potential width parameter within ±5%. For systematics used in Ref. [6] r_0=1.2$(A_c+1)^{1/3}$ (where A_c is mass number of the core); such variation corresponds to variation of nucleon number $A\pm6$ around ^{45}Fe. The sensitivity to a possible deviation of the potential parameters from given by the systematics is significant, but it is not sufficient to change qualitatively our previous conclusion.

IV. THREE-BODY CORRELATIONS

Three-particle decay is completely described by nine parameters (components of three vectors) if we forget about spin degrees of freedom. Three parameters of those are for center of mass translation. Three parameters correspond to an arbitrary rotation of the decay plane (say, three Euler angles), which also contains no useful information for an unpolarized initial state. For narrow states the decay energy E_T can be considered as fixed. Finally, the full correlation information for three-body decay can be described by two parameters. It is convenient to choose the energy distribution $\varepsilon=E_x/E_T$ between subsystems, and the cosine $c_k=\cos(\theta_k)$ of the angle θ_k between Jacobi momenta vectors $\mathbf{k}_x$ and $\mathbf{k}_y$ (see Fig. 7). In these variables the correlation picture is especially indicative. In T Jacobi system parameter ε describes energy distribution between two protons; in Y Jacobi system between core and proton. The Jacobi momenta are defined as

$$\mathbf{k}_x=\frac{A_2\mathbf{k}_1-A_1\mathbf{k}_2}{A_1+A_2},$$

$$\mathbf{k}_y=\frac{A_3(\mathbf{k}_1+\mathbf{k}_2)-(A_1+A_2)\mathbf{k}_3}{A_1+A_2+A_3}, \qquad (1)$$

where $\mathbf{k}_x$ is the momentum of particle 1 in the center of mass (c.m.) of particles 1 and 2, $\mathbf{k}_y$ is the momentum of

c.m. of particles 1 and 2 in the center of mass of the whole system (particles 1, 2, and 3). The convention for labeling of particles is as follows: in the T Jacobi system particle number 3 is core; in the Y system core is either particle 1 or 2. The distribution calculated in definite Jacobi system defines the relative energy spectrum of particles 1 and 2 and correspondingly the single-particle spectrum of 3 ($\mathbf{k}_3=-\mathbf{k}_y$ in the c.m. of the three-body system). The total c.m. energy of the system is easily expressed in terms of Jacobi momenta:

$$E_T = \varkappa^2/2M = E_x + E_y = k_x^2/(2MA_x) + k_y^2/(2MA_y),$$

$$A_x = \frac{A_1A_2}{A_1+A_2}, \qquad A_y = \frac{(A_1+A_2)A_3}{A_1+A_2+A_3}.$$

The distribution of the energy between the subsystems define the hyperangle in the momentum space

$$\theta_\varkappa = \mathrm{arctg}[\sqrt{E_x/E_y}].$$

The Jacobi vectors $\mathbf{X}$ and $\mathbf{Y}$, conjugated to momenta $\mathbf{k}_x$ and $\mathbf{k}_y$, are

$$\mathbf{X} = \mathbf{r}_1 - \mathbf{r}_2, \mathbf{Y} = \frac{A_1\mathbf{r}_1 + A_2\mathbf{r}_2}{A_1+A_2} - \mathbf{r}_3.$$

The hyperspherical variables in the coordinate space

$$\rho^2 = x^2 + y^2, \ \theta_\rho = \mathrm{arctg}[x/y],$$

are expressed via scaled Jacobi vectors $\mathbf{x}=\sqrt{A_x}\mathbf{X}$ and $\mathbf{y}=\sqrt{A_y}\mathbf{Y}$.

In Ref. [2] we were looking for the decay solutions of three-body Hamiltonian (WF with pure outgoing asymptotic). Since the imaginary part of the energy for radioactivity type of solution is very small compared to real part we solved the inhomogeneous equation with real energy

$$(\hat{H}_3 - E_T)\Psi_3^{(+)} = -i(\Gamma/2)\Psi_{\mathrm{box}}. \tag{2}$$

The WF Ψ_{box} is a discrete spectrum solution of the equation

$$(\hat{H}_3 - E_T)\Psi_{\mathrm{box}} = 0 \tag{3}$$

with zero boundary condition at some large (but still under the barrier) hyperradius. The width was found via "physical" definition

$$\Gamma = j/N = j\Big/\left(\int d\Omega_\rho d\Omega_\kappa \int_0^{\rho_{int}} d\rho\rho^5 |\Psi_3^{(+)}|^2\right), \tag{4}$$

where j is a current through the hypersphere of large radius and N is a normalization of the WF inside this sphere ("internal normalization"). The three-body decay WF has the form

$$\Psi_3^{JMSM_S(+)} = \rho^{-5/2}\sum\nolimits_{K\gamma}\chi_{K\gamma}^{(+)}(\varkappa\rho)\mathcal{J}_{K\gamma}^{JM}(\Omega_\rho) \times \sum\nolimits_{M_L} C_{LM_LSM_S}^{JM}\mathcal{I}_{K\gamma}^{LM_L}(\Omega_\varkappa), \tag{5}$$

$$\mathcal{J}_{KLSS_xl_xl_y}^{JM}(\Omega) = [\mathcal{I}_{Kl_xl_y}^{LM_L}(\Omega)\otimes X_{SS_x}]_{JM},$$

where five-dimensional "angles" in the coordinate and in the momentum space are $\Omega_\rho=\{\theta_\rho, \hat{X}, \hat{Y}\}$, $\Omega_\varkappa=\{\theta_\varkappa, \hat{k}_x, \hat{k}_y\}$. This WF is characterized by the total angular momentum J, total spin S, and their projections on the third axis M and M_S. Instead of total spin projection quantum number it can be characterized by spin projections of individual clusters $\Psi_3^{JMM_1M_2M_3(+)}$. Then a summation with Clebsch-Gordan coefficients should be added:

$$\sum\nolimits_{M_{S_x}} C_{S_xM_{S_x}S_3M_3}^{SM_S} C_{S_1M_1S_2M_2}^{S_xM_{S_x}}.$$

Expansion (5) is truncated by the maximal number of the hyperspherical $K_{\max}$ taken into account. X_{SS_x} is the spin function of core and two nucleons with total spin S (two nucleons are coupled to spin S_x),

$$X_{SS_xM_S} = [[\chi_{S_1}\otimes\chi_{S_2}]_{S_x}\otimes\chi_{S_3}]_{SM_s}$$

and

$$\mathcal{I}_{Kl_xl_y}^{LM_L}(\Omega_\rho) = \psi_K^{l_xl_y}(\theta_\rho)[Y_{l_x}(\hat{x})\otimes Y_{l_y}(\hat{y})]_{LM_L}.$$

The hyperangular eigenfunctions $\psi_K^{l_xl_y}$ are proportional to the Jacobi polynomials $P_n^{\alpha,\beta}$,

$$\psi_K^{l_xl_y}(\theta_i) = N_K^{l_xl_y}(\sin\theta_i)^{l_x}(\cos\theta_i)^{l_y}P_{(K-l_x-l_y)/2}^{l_x+1/2,l_y+1/2}(\cos 2\theta_i). \tag{6}$$

The radial components of this WF at large ρ values behave as

$$\chi_{K\gamma}^{(+)}(\varkappa\rho) \sim A_{Ll_xl_y}^{KSS_x}(\varkappa)\mathcal{H}_{K\gamma}^{(+)}(\varkappa\rho), \tag{7}$$

where $\mathcal{H}_{K\gamma}^{(+)}$ are some combinations of Coulomb functions with outgoing asymptotic $(G+iF)$, obtained by diagonalization of Coulomb interaction on the truncated hyperspherical basis at large values of ρ [2]. For sufficiently large ρ values, coefficients $A_{Ll_xl_y}^{KSS_x}$ become independent on ρ. The current through the hypersphere of the radius $\rho=a$ is given by

$$j(a,\Omega_\varkappa) = \frac{1}{M}\mathrm{Im}\int d\Omega_\rho\Psi_3^{(+)\dagger}\rho^{5/2}\left.\frac{d}{d\rho}\rho^{5/2}\Psi_3^{(+)}\right|_{\rho=a}, \tag{8}$$

which allows to define momentum distributions via the asymptotic amplitudes $A_{Ll_xl_y}^{KSS_x}$,

$$\frac{d^2j}{d\varepsilon\, d_{c_k}} = \sqrt{\frac{2E_T}{M}}\sqrt{\varepsilon(1-\varepsilon)}\sum_{LSS_x}\sum_{KK'}\sum_{l_xl_x'l_yl_y'}(A_{Ll_x'l_y'}^{K'SS_x}(E_T))^* \times A_{Ll_xl_y}^{KSS_x}(E_T)\psi_{K'}^{l_x'l_y'}(\theta_\varkappa)\psi_K^{l_xl_y}(\theta_\varkappa) \times \frac{\hat{l}_y'\hat{l}_y}{2L+1}\sum_m C_{l_x'ml_y'0}^{Lm}C_{l_xml_y0}^{Lm}N_{l_x'}^mP_{l_x'}^m(c_k)N_{l_x}^mP_{l_x}^m(c_k), \tag{9}$$

where $N_{l_x}^mP_{l_x}^m(c_k)$ are the Legendre polynomials normalized to unity.

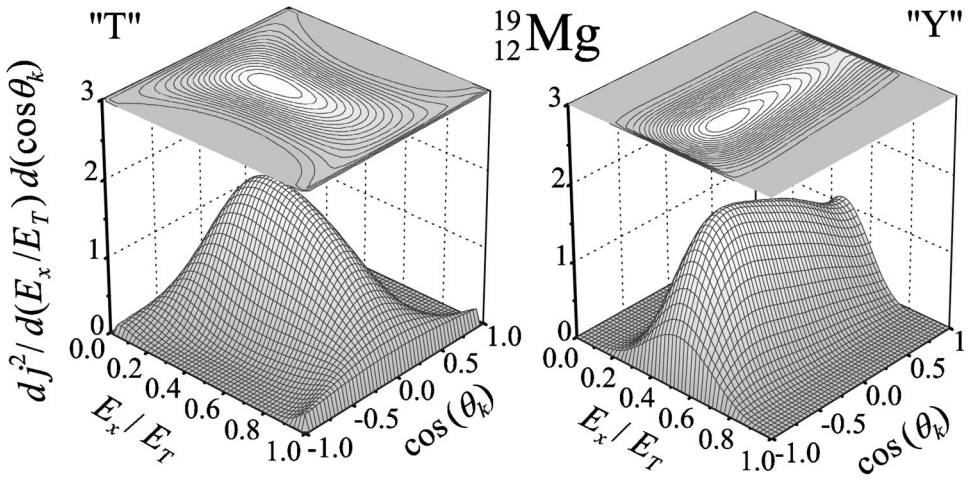

FIG. 8. Correlations for the ^{19}Mg decay in T and Y Jacobi systems. Calculations from Ref. [5], case of a strong *s*/*d* mixing (~60% of *s* wave, E_T= 580 keV).

Some words of caution are required here. The fact that the hyperradius itself is large does not guarantee that all interparticle distances are large and hence that the asymptotic region is achieved for motion of all particles. There are places on the hypersphere, where particles are close to each other even for a hyperradius tending to infinity. The success of the method we use for "true" two-proton emission is defined by the fact that in such decays the particles rapidly leave the regions where they are close to each other after they leave the Coulomb barrier region. This happens due to strong Coulomb repulsion and absence of the long-living states in the subsystems energetically available for decay. Technically this happens due to formation of the specific correlations, which we are going to consider (Secs. IV A and IV B). In such a case the large ρ values appear to have direct relation with large intercluster distances. The independence of the distribution (9) on the hyperradius ρ means that there is no redistribution of energy and momentum among particles any more. The motion of the system solely along hyperadial direction means that the system is simply "inflating" as time goes; this is a signal that the asymptotic regime is achieved. The stability of momentum distributions obtained by means of Eq. (8) is specially discussed in Sec. IV C.

A. General features

The full correlation picture is presented in Figs. 8 and 9 for selected cases of the internal structure for ^{19}Mg and ^{45}Fe

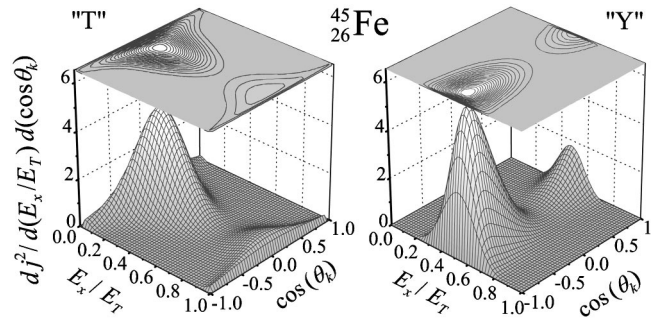

FIG. 9. Correlations for the ^{45}Fe decay in T and Y Jacobi systems. Case of the *f*-wave domination (~75% of *f* wave, E_T =1140 keV).

decays. The following common features of the correlations in the 2*p* decay can be illustrated by these examples.

(i) The particles are blown out from kinematics regions $\{\cos(\theta_k)=\pm 1, E_x/E_T \sim 0.5\}$ in the T system. These conditions correspond to the situation when the core and one of the protons are flying out with close velocity vectors (and hence residue in the region of strong Coulomb repulsion for a long time). This effect is more expressed in ^{45}Fe, where the Coulomb interaction is much stronger.

(ii) In the T system the particles are predominantly in the T-like configurations $[\cos(\theta_k)\sim 0]$, which are likely to expand as a whole, without change of relative distances (this corresponds to the motion of the system entirely along ρ variable in hyperspherical coordinates).

(iii) In Y Jacobi system the same physics as in (i) and (ii) is reflected by concentration of particles at $E_x/E_T \sim 0.5$. The distributions projected on the $\varepsilon = E_x/E_T$ axis have a narrow practically symmetric peak. They are shown in Fig. 10 for a number of 2*p* emitters. It is easy to notice that the heavier the system is, the narrower is the distribution. The width of this distribution is not changing with the charge monotonously because there is another factor, influencing the width of the distribution, namely, the 2*p* decay energy E_T. For the shown distributions the E_T value varies from 0.7 MeV in ^{19}Mg to 2.8 MeV in ^{62}Se. The behavior of these distributions is in an agreement with general prediction of Goldansky [7] that in the case of true two-proton emission the protons should have close energies.

(iv) Some hint about Coulomb repulsion in the *p*-*p* pair can also be found in Figs. 8 and 9. In energy distribution between protons the evidence is quite small due to small Coulomb interaction compared to Coulomb interaction in the core-*p* subsystem (10–30 times stronger). However, in angular distributions the fingerprints are quite evident: there is a fall in the probability at $\cos(\theta_k)=-1$ (in Y system). This angle corresponds to the situation when both protons are flying in the same direction.

(v) There is a strong qualitative difference between correlations in the decays of *s*-*d* and *p*-*f* shell nuclei. The *p*-*p* energy distributions calculated for different *s*-*d* nuclei in different assumptions about *s*/*d* mixing nevertheless look very similar, see Fig. 11. The same distribution calculated in *p*-*f*

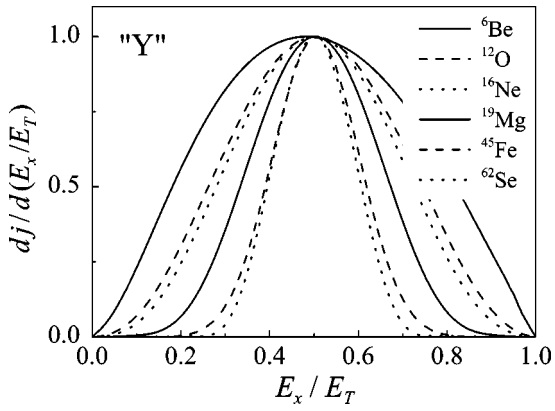

FIG. 10. The energy distributions between the core and one of the protons for several nuclei (Y Jacobi system). Two-proton decay energies E_T are 1.37, 1.79, 1.4, 0.8, 1.15, 2.8 MeV for ^{6}Be, ^{12}O, ^{16}Ne, ^{19}Mg, ^{45}Fe, and ^{62}Se, correspondingly. It is possible to notice that the distribution for ^{6}Be is slightly asymmetric, which is connected with a small mass of core.

nuclei strongly depend on the p/f ratio, see Fig. 12. More detailed discussion of this issue follows.

(vi) The dependence of the observed correlations on the total decay energy E_T is quite small. In Fig. 13 this is illustrated on the example of ^{45}Fe. The correlations are shown for energies from 0.7 to 3.3 MeV (the width varies from about 10^{-28} to about 10^{-8} MeV). As the energy grows (and the width of the Coulomb barrier decreases) the core-p energy distribution becomes broader. This is a generally expected result. The width of the distribution over $\cos(\theta_k)$ in the T system also grows with energy. The "diproton" peak ($\varepsilon \ll 1$) in T system drift to lower ε values. However, it should be understood that the energy of the p-p peak in reality grows: it is about 90 keV for E_T=0.7 MeV and about 300 keV for E_T=3.3 MeV.

B. Decay mechanisms

The strong qualitative difference can be found between correlations in the decays of ^{19}Mg and ^{45}Fe in distributions over ε in the T system (Figs. 8, 9, 11, and 12). This difference is also clearly reflected in the distributions over $c_k = \cos(\theta_k)$ in the Y system. We have found that this kind of correlation is stable in the s-d shell nuclei (for ^{12}O and ^{16}Ne see Ref. [3], and Ref. [5] for ^{19}Mg) with respect to a variation of the s/d ratio. When we change the s/d ratio drastically the variations in the distributions are rather quantitative than qualitative.

This appear to be not true for the p-f shell nuclei. The variation of the distribution over ε in the T system with variation of the p/f ratio for ^{45}Fe is shown in Fig. 12. In the

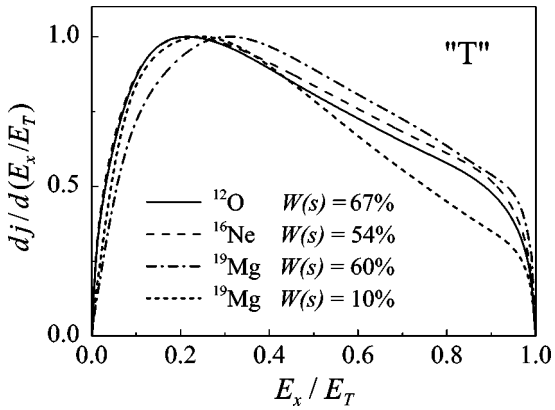

FIG. 11. The energy distributions between two protons (T Jacobi system) in different s-d shell nuclei.

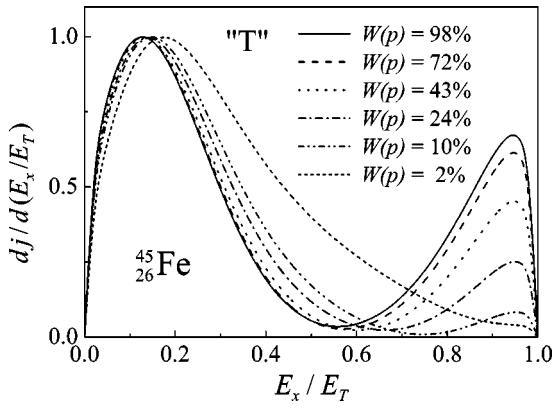

FIG. 12. The energy distributions between two protons (T Jacobi system) in different assumptions about internal structure of ^{45}Fe. $W(p)$ is the weight of the p^2 configuration in the nuclear interior.

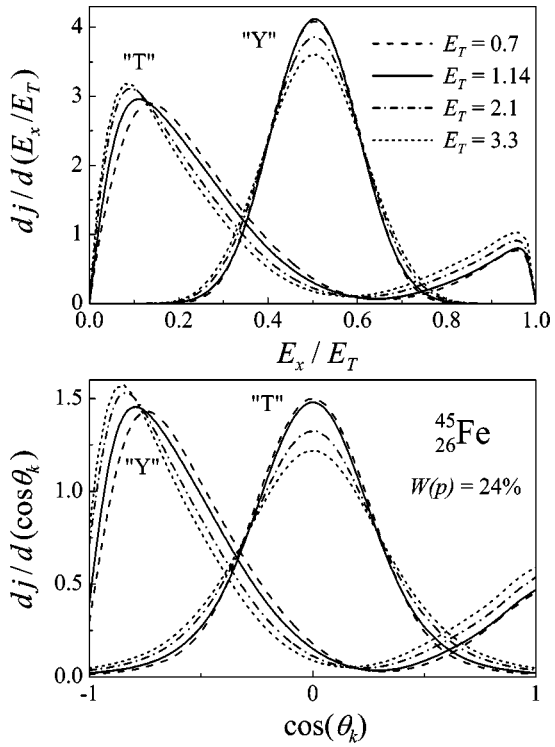

FIG. 13. The energy and angular distributions for ^{45}Fe as a function of the decay energy E_T. The letters T and Y near the bunches of curves indicate in which Jacobi system the distribution is calculated.

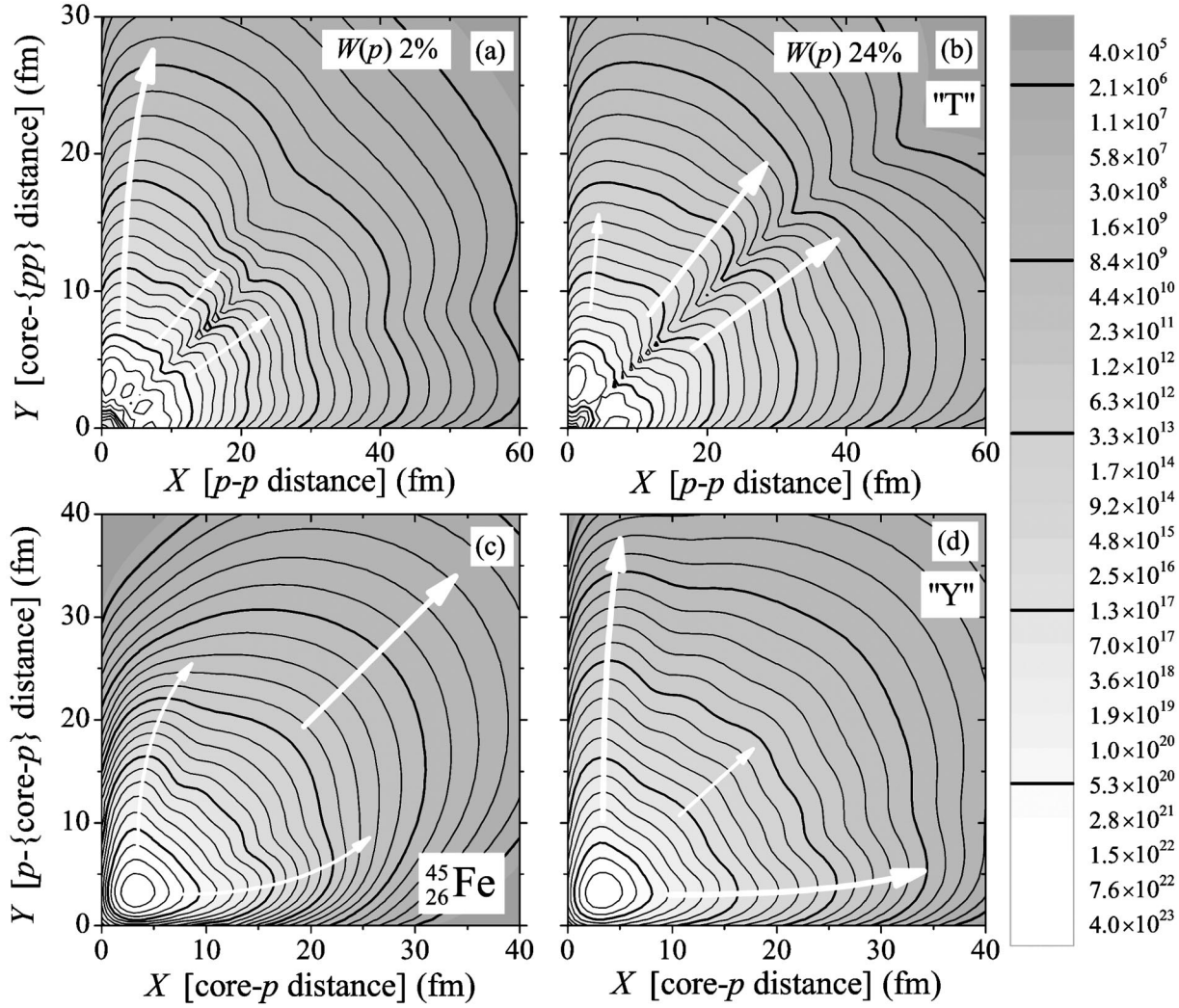

FIG. 14. WF density $|\Psi_3^{(+)}(X,Y)|^2$ plots for subbarrier region illustrating difference in decay mechanisms for two cases of ^{45}Fe structure. The WF is normalized for integration over $dX\,dY$. Left column shows case $W(p)=2\%$; right column shows case $W(p)=24\%$. First and second rows correspond to T and Y Jacobi systems. Thick and thin white arrows indicate dominating and auxiliary decay paths. Diproton path is dominating in (a) and (c) and "sequential" in (b) and (d).

case of the f^2 domination this distribution has a single broad peak at low p-p energy (diproton peak which is strongly connected with the p-p final state interaction). This tells that in the subbarrier region the protons first move from f^2 to s^2 configuration and only then tunnel. For that reason they "forget" about complicated correlations typical for f^2 component in the nuclear interior [see Fig. 14(a)].

In Refs. [1,2] we have drawn a conclusion about "washing out" of the correlations typical to nuclear interior during the decay on the basis of studies of nuclei with s/d mixing and f-wave domination. It appears, however, that in the case of a considerable p/f mixing the dynamics changes abruptly. In that case the protons are tunneling directly from the p^2 configuration with only a minor contribution of the s^2, which is reflected in a double-hump structure of the spectrum. A qualitatively similar double-humped spectrum has already been observed experimentally in the $2p$ decay of the p-wave nucleus ^{6}Be [19] and is probably well understood (see calculations in Ref. [4]). It is interesting to note that this similarity exists also for the decays of the p-wave nuclei on the neutron dripline [17].

We can see in Fig. 12 how the energy distribution evolves for ^{45}Fe with the increase of the p^2 configuration, and, in Fig. 6(a), how this evolution is correlated with changes of the lifetime. Interesting feature of the correlations is the fact that for very different energy correlations in the T system (the p-p distribution over E_x, Fig. 12), the core-p distribution in the Y system remains the same (see Fig. 10).

The above speculations about mechanisms of penetration are illustrated in Table I. The table shows, which HHs contribute to the structure (internal region) and decay (asymptotic region) for the cases of ^{19}Mg and ^{45}Fe. To interpret this Table it is useful to know that s^2, p^2, d^2, and f^2 shell-model configurations are closely related with HHs with $\{LS_x l_x l_y\}=\{0000\}$ and K equal 0, 2, 4, and 6, respectively. It should be noted that only in very special cases there is (at least) some correspondence between components important in the interior and components playing role at the asymptotic. In the general case the redistribution of weights in the process of decay is absolutely essential.

The importance of the "diproton" decay mechanism shows itself as strong contribution of $K=0$ component to the

TABLE I. Contributions of different HH components of the WF into internal normalizations N_i and partial widths Γ_i, see Eq. (4). Only components contributing significantly are selected. For N_i integration is up to ρ_{int}=18 fm. The internal normalizations and relative partial widths Γ_i/Γ are in percent. Cases of ^{19}Mg (~60% of *s* wave and ~10% of *s* wave), ^{45}Fe (~2%, ~24%, and ~98% of *p* wave). Dominating components are given in bold font. Total spin *S* is everywhere 1/2 for ^{19}Mg and 3/2 for ^{45}Fe.

Component					^{19}Mg, $W(s)$=10%		^{19}Mg, $W(s)$=60%		^{45}Fe, $W(p)$=2%		^{45}Fe, $W(p)$=24%		^{45}Fe, $W(p)$=98%	
K	L	S_x	l_x	l_y	N_i	Γ_i/Γ	N_i	Γ_i/Γ	N_i	Γ_i/Γ	N_i	Γ_i/Γ	N_i	Γ_i/Γ
0	0	0	0	0	6.9	**66.0**	**56.8**	**67.3**	0.45	**47.9**	0.79	11.1	0.9	2.5
2	0	0	0	0	4.2	3.1	3.7	0.4	0.77	12.4	23.3	**46.7**	**96.3**	**62.9**
2	1	1	1	1	5×10^{-5}	3×10^{-6}	2×10^{-3}	2×10^{-6}	1×10^{-5}	2×10^{-3}	0.1	0.5	15.9	3.1
4	0	0	0	0	**80.1**	1.1	37.9	1.1	0.63	2.7	0.9	1.4	0.4	1.0
4	0	0	2	2	5.8	25.9	0.3	27.4	2×10^{-5}	25.5	5×10^{-4}	8.1	4×10^{-3}	1.8
6	0	0	0	0	0.1	0.3	0.1	0.3	**73.4**	0.9	**58.7**	1.6	0.3	1.8
6	0	0	2	2	4×10^{-2}	0.4	4×10^{-2}	7×10^{-2}	15.9	4.8	11.5	18.5	0.45	21.2
8	0	0	2	2	0.7	0.5	0.5	0.5	1×10^{-3}	1.2	1×10^{-3}	0.8	5×10^{-4}	0.2
8	0	0	4	4	0.3	2.6	8×10^{-3}	2.8	3×10^{-3}	3.4	2×10^{-3}	2.7	7×10^{-5}	0.3
10	0	0	4	4	2×10^{-4}	1×10^{-2}	2×10^{-3}	4×10^{-3}	0.3	0.5	0.2	3.6	9×10^{-3}	2.2

decay width. One can see that for ^{19}Mg (representative of *s-d* shell nuclei) the domination of the K=0 component in the width is independent on the internal structure. For ^{45}Fe (as representative of *p-f* shell nuclei) this component is dominating in the decay only in the extreme case of a pure f^2 internal structure.

Also a hint about decay mechanisms can be obtained from the WF density distributions in the barrier region. In Fig. 14 two cases of ^{45}Fe calculations are shown: $W(p)$=2% (*f*-wave domination) and $W(p)$=24% (significant *p*/*f* mixing). In the first case one can see in the T system a strong "ridge" at small X distances [Fig. 14(a)]. This corresponds to small distances between two-protons and hence a strong diproton decay mechanism. In second case [Fig. 14(b)] this "ridge" can hardly be seen. However, in second case we see two symmetric ridges in the Y coordinate system at small X and small Y distances [Fig. 14(d)], which correspond to importance of core-*p* correlation. This is a kind of "sequential" decay mechanism, with exception that resonances in the subsystems have much shorter lifetimes than the three-body system and hence decay under the barrier. They nevertheless can contribute width as virtual excitations [what we can actually see in Fig. 14(d)]. In the first case these ridges are also noticeable [Fig. 14(c)], but they rapidly dissolve and thus do not contribute the width significantly.

What we see in Fig. 14 is a nice illustration, how competition between different kinds of dynamics leads to transitions between different decay mechanisms. It is also clear that in our model no assumption is done about importance of this or that decay mechanism, both mechanisms are present simultaneously and it is three-body Hamiltonian, that "chooses" the right dynamics in each case.

C. Convergence of momentum distributions

As mentioned above, we use the approximate asymptotic of the Coulomb problem for three particles [2]. Thus, when we work with momentum distributions of the decay products, the reliability of these approximations should be understood. We are going to discuss convergence of momentum distributions for the example of one selected calculation for ^{45}Fe.

Figures 15 and 16 demonstrate remarkable stability of our calculations. Figure 15 shows how the momentum distributions depend on the integration radius $\rho_{\max}$ (radius at which the solution is matched to the asymptotic). At $\rho_{\max}$ ~500–600 fm the distributions become stable. The modification of distributions with increase of $\rho_{\max}$ up to 1000 fm is on the level of numerical precision of our calculations. Such stability shows clearly that there is no redistribution of energy among particles and the motion of the system is just inflation. In hyperspherical coordinates it corresponds to the motion solely along ρ variable. Similarly the convergence with respect to the size of the hyperspherical basis seems to be achieved (see Fig. 16). The distributions starting from $K_{\max}$=16 are indistinguishable within numerical precision. Relatively rapid convergence of the calculations with respect to $K_{\max}$ is an expected feature of the true two-proton decays. By definition of such decays there are no long-living resonances in the subsystems (energetically available for decay). Then, due to Coulomb repulsion in each pair the particles rapidly leave the regions, where their motion is strongly correlated. So, the resulting three-body amplitudes should be smooth and thus easily expandable in the hyperspherical space. This is exactly the kind of picture one finds in Figs. 8 and 9 the momentum distributions are smooth, without any really sharp features, and the particles are blown out from the regions, where they are close to each other. It should also be noted that while the huge radii $\rho_{\max}$~700 and huge basis sizes $K_{\max}$~20 are required to achieve the full convergence of the distributions, all the gross features are already present in much more compact calculations with $\rho_{\max}$~300 and $K_{\max}$~8 and improvements achieved in a very bulky calculations are quantitative, not qualitative.

The good convergence of the results demonstrated in Figs. 15 and 16 cannot be a rigorous proof of the convergence in the case of long-range Coulomb interaction. There is no reliable mathematical proof that a large number of additional

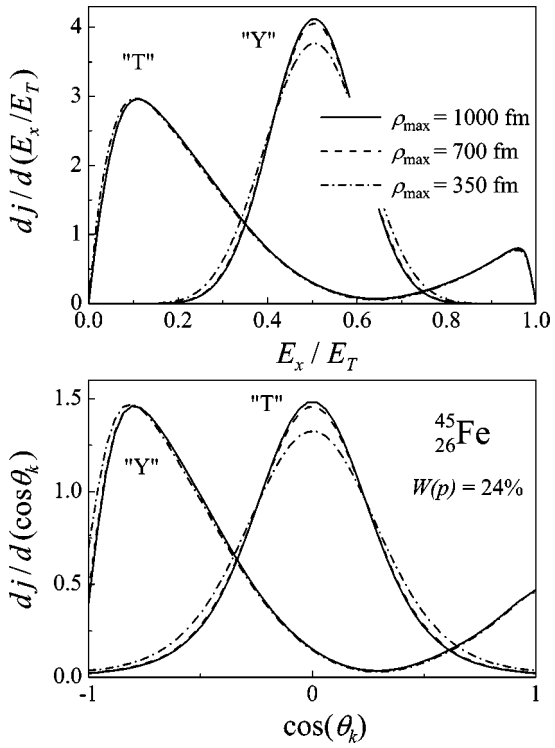

FIG. 15. The energy and angular distributions for ^{45}Fe as a function of integration radius ρ_{max}.

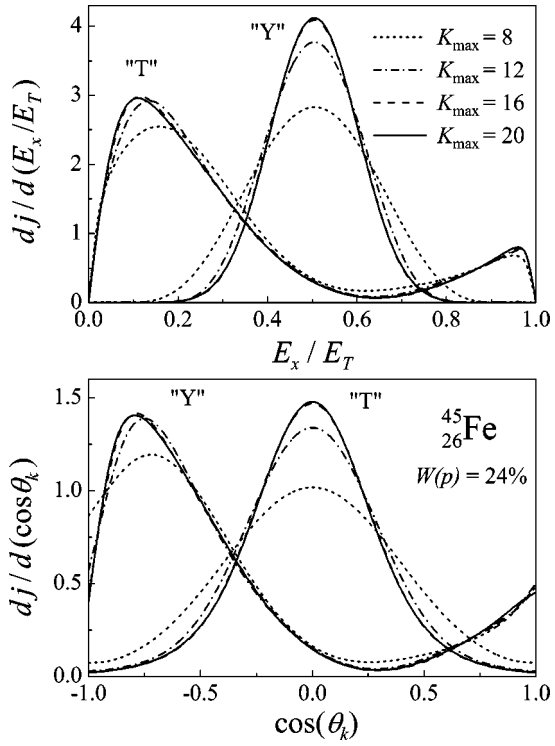

FIG. 16. The energy and angular distributions for ^{45}Fe as a function of K_{max} in T and Y Jacobi systems.

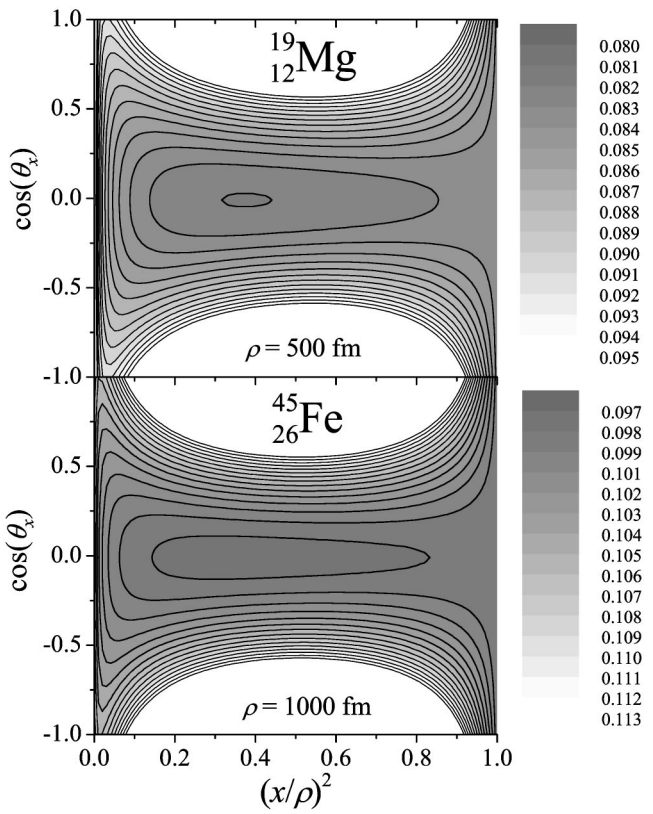

FIG. 17. Coulomb potential surfaces for ^{19}Mg and ^{45}Fe at large values of ρ in the T Jacobi system. Contours are given with 1 keV step.

components would not lead to a significant modification of the obtained distributions. In justification of our results we appeal to physical common sense. As we have seen in Fig. 15 the motion of particles is practically entirely inflation. In this case the momentum distribution calculated at ρ_{max} closely corresponds to spatial distribution at $\rho=\rho_{max}$. In Fig. 17 the Coulomb potential surfaces at constant ρ are given for variables $(x/\rho)^2$ and θ_x which correspond to ε and θ_k of momentum representation. Comparison with Figs. 8 and 9 shows that particles are concentrated in the regions of $\{\varepsilon, \cos\theta_k\}$ plane (or what is approximately the same of $\{(x/\rho)^2, \cos\theta_x\}$ plane), where the Coulomb potential (at given ρ) has a very flat minimum. The Coulomb potential itself is still not negligible at maximal ρ_{max} values achieved in our calculations. Say, for ^{45}Fe at ρ_{max}=1000 fm it is around 100 keV in the minimum. This is about 10% of the decay energy of ^{45}Fe (1.14 MeV). However, the variation of the Coulomb potential in the region of $\{(x/\rho)^2, \cos(\theta_x)\}$ plane, where 98% of the WF residue does not exceed 5–10 keV. So, the part of the remaining Coulomb energy, which can lead to redistribution of energy among the particles is really very small. For that reason the expectation is that the majority of the remaining Coulomb energy will be pumped into inflation motion of the system.

The simple way to estimate the possible influence of the "residual" Coulomb interaction on the obtained momentum distributions is to make a classical extrapolation of these distributions. Such extrapolation is shown in Fig. 18 for ^{45}Fe

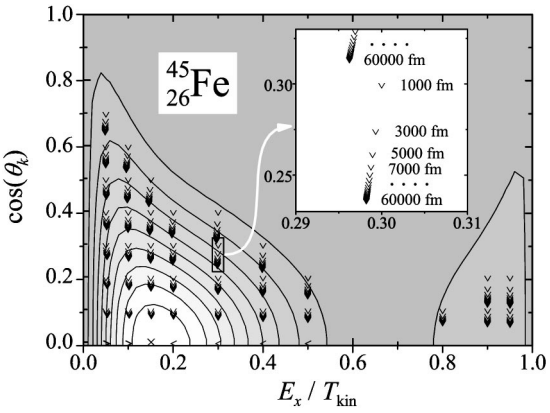

FIG. 18. Classical extrapolation of the momentum distribution for ^{45}Fe. The contour map in the background shows the momentum distribution at ρ=1000 fm (see Fig. 9). Evolution of momentum correlations along classical trajectories is shown by sequences of angles. The angles come with step of 2000 fm and show the direction of evolution. First angle of every sequence corresponds to point on hypersphere ρ=1000 fm with definite momenta. Each sequence shows in which part of momentum space the classical trajectory ends. T_{kin} is the kinetic energy in each point of the trajectories. In the inset one selected trajectory is shown on a large scale.

case. For the point on the hypersphere of the maximal hyperradius $\rho=\rho_{max}$ achieved in the quantum mechanical calculations a set of momenta can be defined via derivatives of the decay WF. This provides initial conditions for classical trajectory calculation. If the initial point residue in the classically allowed region, then there are no problems with complex momenta and hence classical trajectories are well motivated. As we can see from Figs. 9 and 17 this condition is satisfied with a good precision: the WF at achieved large hyperradius is already practically entirely in the classically allowed region. For ^{45}Fe the reasonable distance for classical trajectory calculations, after which the momentum distributions stabilize, is $(3–6)\times10^4$ fm in hyperradius.

Classical extrapolation (Fig. 18) shows that qualitative speculations based on Fig. 17 seem to be reasonable. Practically no energy redistribution is happening in the T system. There is a modification of the distribution on $\cos(\theta_k)$ variable. One can estimate that this distribution should become 10–20% narrower. Correspondingly the distribution over ε in the Y Jacobi system should also become somewhat narrower. Classical extrapolation indicates possible significant modifications only for the parts of momentum space where a very small part of the WF residue.

So, no qualitative change of our results is expected in general and no modification of energy distribution in the T system is expected at all.

The academic question about convergence of momentum distributions remains open and deserve further studies. Precision calculations of all distributions require to go very far in radius; for "typical" 2p emitter, like ^{45}Fe, they seem to stabilize completely at hyperradii of tens of thousands of fm. However, from a pragmatic point of view the problem is solved to the practically required precision. Expected theoretical uncertainty due to approximate character of the boundary conditions is incomparably smaller than theoretical uncertainty associated with other things (say, nuclear structure; see Fig. 12, for example). Any experimental data, available at the moment or expected in the observable future, are also incomparably less precise than required to put restrictions on this kind of theoretical uncertainty. It should be noted that the complicated issues of radial convergence of the distributions have nothing in common with convergence of width. For example, for the discussed case of ^{45}Fe calculation integration of equations up to $\rho_{max}\sim150–250$ fm is sufficient to stabilize the width [2].

D. Projected distributions

In experiments an incomplete kinematics information is often obtained. For example in schematic experimental setups discussed in Refs. [5,16] the tracking procedure may be able to provide only trajectories of the decay fragments, not the energies. Thus only the momentum projections on one plane can be measured, i.e., the distributions are integrated over one dimension. It is an interesting question to which extent the valuable part of information remains after such integration.

In Figs. 19 and 20 the projected momentum distributions for ^{19}Mg and ^{45}Fe are shown, calculated in three different models. The three-body calculations are presented in Section IV A (see Figs. 8 and 9).

Comparison with phase volume is a standard way to define the existence of specific correlations in the system. The s-wave phase volume for three particles is given by

$$dj/d\varepsilon \sim \sqrt{\varepsilon(1-\varepsilon)}.$$

In the standard diproton model the zero energy of relative motion between two protons is implied (see diproton model curves in Figs. 1–5. In this form the diproton model provides the upper limit for the 2p emission width [6], but it cannot give momentum distributions. To model momentum distribution the experimentalists ordinarily use the diproton model in the form

$$dj/d\varepsilon \sim P_0(\varepsilon E_T, 1, r_{ch}(pp)) \times P_0((1-\varepsilon)E_T, 2Z_c, r_{ch}(\text{core-}\{pp\})),$$

which gives energy distribution, but not the width. Here parameter ε describe the energy distribution in the T Jacobi system, and $P_l(E, Z_1Z_2, r_{ch})$ is a standard two-body penetrability depending on the relative energy of the particles, charges, and channel radius. The channel radius parameters are $r_{ch}(pp)=2.5$ fm, $r_{ch}(\text{core-}\{pp\})=5.55$ fm for ^{19}Mg and $r_{ch}(\text{core}-\{pp\})=6.91$ fm for ^{45}Fe (see Ref. [6]). We do not consider the diproton model as a realistic alternative to the three-body calculations. However, it remains popular in the literature in different modifications [15,20] and methodologically such comparison is desirable.

From Figs. 19 and 20 one can see that different models are distinguishable even after integration over one variable. Some distributions can be quite close, but there are always some distributions, which are qualitatively different. This fact emphasizes the necessity to perform model comparison

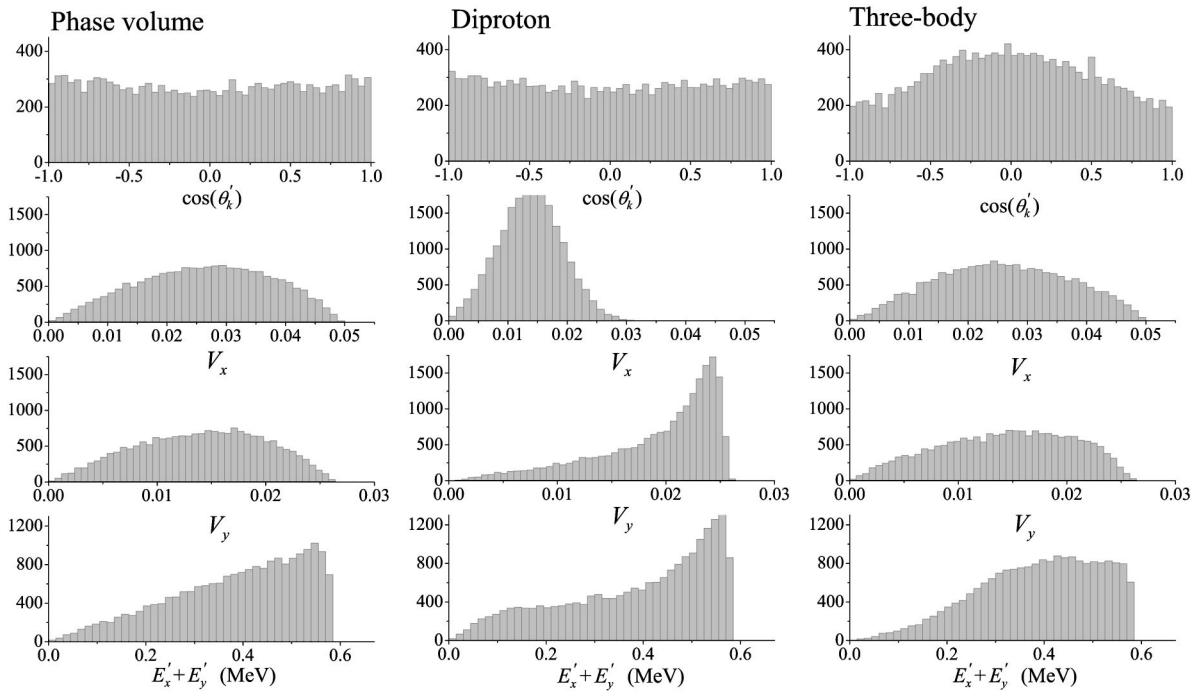

FIG. 19. The Monte Carlo simulation (20 000 events, *y* axis show number of events) of projected on the plane distributions for ^{19}Mg (for original three-body distribution see Fig. 8, E_T=580 keV). V_x and V_y are Jakobi velocities (in the T system) projected on the plane in the units of speed of light. The angle θ_k' here is also angle between projected vectors $\cos(\theta_k')=(\mathbf{V}_x, \mathbf{V}_y)/V_xV_y$. E_x' and E_y' are the energies associated with the projected velocities.

with experiment for several distributions simultaneously, as some of them can coincide by chance.

What distinguishes the three-body model significantly both from diproton model and phase volume is the distribution over $\cos(\theta_k')$. The shape of this distribution clearly reflects much sharper focusing over angle θ_k in the complete three-dimensional distributions of Figs. 8 and 9. This feature is defined by complicated dynamics of the three-body motion in the three-body Coulomb potential and is not present in the simple approximations.

It is important that the projected spectra provide a reliable way to determine the decay energy: in all models the distri-

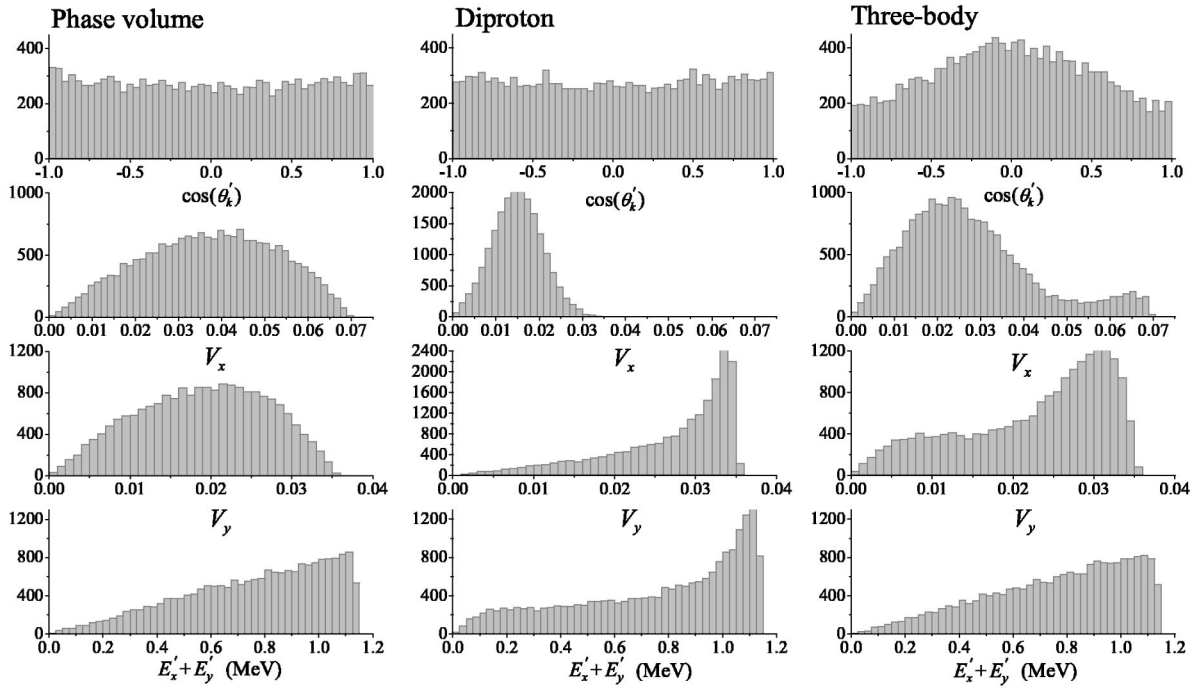

FIG. 20. The Monte Carlo simulation of projected on the plane distributions for ^{45}Fe (for original three-body distribution see Fig. 9, E_T=1140 keV). See the caption of Fig. 19 for details.

TABLE II. Nuclei with $A \leqslant 71$, predicted to be true two-proton emitters (but not yet observed). $E_T = -S_{2p}$ is the energy above the two-proton breakup threshold (corresponding width or lifetime range is shown in the ninth column). S_p is the proton separation energy. Spin parities for the nucleus, ground state in core+p subsystem and the core are given in second, fifth, and eights columns. Quantum numbers J^π in the brackets are assumed.

${}^{A}_{Z}Z$	J^π	E_T(keV)	${}^{A-1}_{Z-1}(Z-1)$	J^π	S_p(keV)	${}^{A-2}_{Z-2}(Z-2)$	J^π	$T_{1/2}$ or Γ	Reference
${}^{19}_{12}$Mg	$(1/2^-)$	1200	${}^{18}_{11}$Na	1^-	2300	${}^{17}_{10}$Ne	$1/2^-$	0.2–6 eV	[8]
		900			600			0.007–0.1 ps	[21]
		500						0.5–7 ns	[22]
		580–860			200–400			0.2–700 ps	[5]
${}^{30}_{18}$Ar	(0^+)	1430	${}^{29}_{17}$Cl	$(3/2^+)$	350	${}^{28}_{16}$S	0^+	0.7–33 ps	[23]
		3105			465			2–26 eV	[24]
${}^{34}_{20}$Ca	(0^+)	755	${}^{33}_{19}$K		900	${}^{32}_{18}$Ar	0^+	0.2–7 ms	[23]
		2190			230			0.1–0.003 ps	[24]
${}^{38}_{22}$Ti	(0^+)	960	${}^{37}_{21}$Sc	$(7/2^-)$	1030	${}^{36}_{20}$Ca	0^+		[23]
		2432			438				[25]
		2590			375				[24]
${}^{41}_{24}$Cr		2249	${}^{40}_{23}$Va	(2^+)	264	${}^{39}_{22}$Ti	$3/2^+$		[10]
${}^{42}_{24}$Cr	(0^+)	498	${}^{41}_{23}$Va	$(7/2^-)$	1216	${}^{40}_{22}$Ti	0^+		[10]
		260			1060				[23]
		−960–1900							[11]
		452			1282				[25]
		655			1150				[24]
${}^{48}_{28}$Ni	(0^+)	1357	${}^{47}_{27}$Co	$(7/2^-)$	469	${}^{46}_{26}$Fe	(0^+)	0.3–9 ms	[10]
		−440–1970						>7 ns	[11]
		1354			479			0.5–15 ms	[26]
		1290			505			3–75 ms	[27]
${}^{54}_{30}$Zn	(0^+)	1510	${}^{53}_{29}$Cu	$(3/2^-)$	400	${}^{52}_{28}$Ni	0^+	0.5–25 ms	[23]
		1794			−153			2–90 μs	[26]
		1873			−230			0.5–25 μs	[27]
		1330			120			40 ms–3.5 s	[28]
${}^{58}_{32}$Ge	(0^+)	2780	${}^{57}_{31}$Ga	$(1/2^-)$	−240	${}^{56}_{30}$Zn	0^+	0.1–6.5 ns	[23]
		2636			−296			0.4–26 ns	[27]
		2380			−160			8–400 ns	[28]
${}^{59}_{32}$Ge	$(7/2^-)$	1100	${}^{58}_{31}$Ga	(2^+)	300	${}^{57}_{30}$Zn	$(7/2^-)$	>2500 s	[23]
		1343			58			>3 s	[27]
		1160			190			>300 s	[28]
${}^{62}_{34}$Se	(0^+)	2888	${}^{61}_{33}$As	$(3/2^-)$	−142	${}^{60}_{32}$Ge	(0^+)	0.4–16 ns	[27]
		2760			−100			1.4–55 ns	[28]
${}^{63}_{34}$Se	$(3/2^-)$	1530	${}^{62}_{33}$As	(1^+)	69	${}^{61}_{32}$Ge	$(3/2^-)$	0.3–15 s	[27]
		1510			110			0.6–27 s	[28]
${}^{66}_{36}$Kr	(0^+)	2832	${}^{65}_{35}$Br	$(5/2^-)$	−1	${}^{64}_{34}$Se	(0^+)	6–400 ns	[27]
${}^{67}_{36}$Kr	$(3/2^-)$	1538	${}^{66}_{35}$Br	(0^+)	155	${}^{65}_{34}$Se	$(3/2^-)$	>15 s	[27]
		1760			−50			46 ms–4 s	[28]
${}^{71}_{38}$Sr	$(5/2^-)$	2060	${}^{70}_{37}$Rb	(4^+)	−20	${}^{69}_{36}$Kr	$(5/2^-)$		[28]

butions over "projected" energy $E_x'+E_y'$ (associated with projected velocities) have sharp end points at maximal available in the decay energy E_T.

V. OVERVIEW AND DISCUSSION

Here we would like to summarize the status of prospective candidates for 2p emission studies, basing on our calculations here, as well as on the previous papers [1–3,5,6]. We should remind once more that the conclusions here depend strongly on the decay energy predictions (see compilation in Table II), which are mostly out of our control and which are implied below to be reliable without further discussions.

The calculation results for various 2p emitters (see Refs. [3–6] and Figs. 2–5) are collected in Fig. 21. They are shown opposite to the lifetime bands accessible (or not accessible) for different experimental techniques. This figure aims to give an overall impression about status of the field on a large scale: from million electron volt of width to seconds of the lifetime.

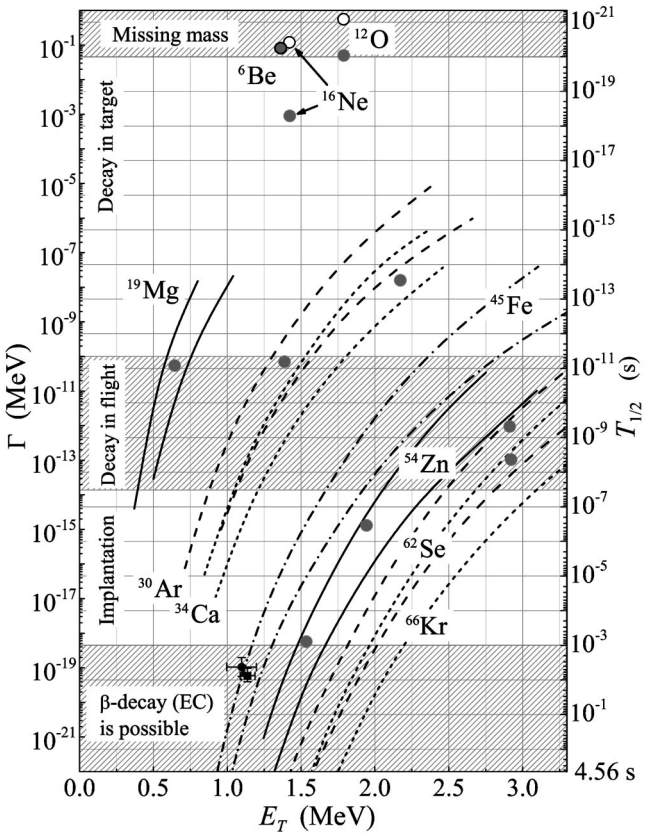

FIG. 21. The lifetimes of various 2*p* emitters and possible experimental techniques. For nuclei from ^{19}Mg to ^{66}Kr "lifetime corridors" are shown for each nucleus by two curves of the same style (^{48}Ni and ^{58}Ge cases are omitted not to crowd the plot). The open circles show experimental widths for ^{6}Be, ^{12}O, and ^{16}Ne. Gray circles stand for calculated values. For heavier nuclei they are quite uncertain and are given more to guide the eye. Open and gray circles overlap in the case of ^{6}Be. Experimental data [14,15] on ^{45}Fe are given as dots with error bars.

In Table II the calculation results for *prospective* (not yet observed) 2*p* emitters are also given opposite to various decay energy predictions. The condition defining that the decay mode is really true two-proton emission is

$$E_T > 0, S_p > 0 \tag{10}$$

(see Refs. [2,7]). What we find in Table II is that for some candidates proton separation energy S_p is negative (hence sequential decay is possible). However, it was shown in Ref. [6] that in reality the sequential decay is beginning to play a significant role only when

$$-S_p > (0.15 - 0.20) \times E_T \tag{11}$$

and strict condition Eq. (10) of Ref. [7] can be relaxed. The weaker condition Eq. (11) is well satisfied for all selected nuclei.

Below we provide a brief summary for the studied 2*p* emitters.

^{6}Be, ^{12}O, ^{16}Ne. The existence of the true two-proton emission phenomenon in these nuclei cause no doubts. However, we think that these systems are far from been sufficiently studied. Complete decay information have not been measured for ^{6}Be (only restricted kinematics regions [19]). Complete decay information have been measured for ^{12}O [29], but not presented in the form making possible the detailed theoretical analysis (see Ref. [17] as example of what we think is a right presentation). In ^{16}Ne the 2*p* emission have never been directly observed. From methodological point of view the detailed studies (full correlations picture) of these systems are very desirable. Special issue is possibility of specific dynamics in ^{12}O and ^{16}Ne predicted in Ref. [3].

^{19}Mg. The predicted lifetime range partly corresponds to decay in flight and partly to decay in target. Predictions of Ref. [5] on this issue connect this variation with *s*/*d* mixing ratio and with possible specific mechanism (we call it three-body mechanism [3]) of Thomas-Ehrman shift. The studies of this nucleus should be of great importance for understanding of these issues.

^{30}Ar. Energy from Ref. [23] puts the ^{30}Ar lifetime in the decay-in-flight range. Systematics [24] provides much shorter lifetimes (decay in the target range).

^{34}Ca. Prediction of systematics [24] corresponds to decay of this nucleus in the production target with no possibility of lifetime derivation. Energy predicted by Ref. [23] can possibly be excluded for this nucleus due to its nonobservation in the fragmentation experiment. This conclusion is based, however, on the unpublished result [30] (see also Ref. [6] for more details). The question is clearly important for understanding of possibilities for ^{30}Ar studies.

^{45}Fe. The recent experimental achievements are very encouraging [14,15]. Agreement with three-body model predictions is very reasonable. However, to discriminate further within the model uncertainty much more precise information about lifetime and decay energy is required. Correlation information would also be very helpful.

^{48}Ni. This nucleus has been observed recently in the fragmentation experiment [31] in a very small amount. The fact of observation allowed to deduce the lower limit for the lifetime; no identification of decay mode was possible. The nucleus is expected to have comparable properties with ^{45}Fe. However, according to calculations, this nucleus residue in the range, where weak decays contribute the lifetime on the level comparable with 2*p* emission. This means that minor variation of expected characteristics can easily bring the nucleus to the range, where 2*p* emission is suppressed.

^{54}Zn. Available decay energy predictions [23,26–28] differ significantly, but for all of them the expected lifetime is entirely within the implantation range. This is a very "reliable" candidate for implantation experiment studies.

^{58}Ge, ^{62}Se, ^{66}Kr. These nuclei seem to be accessible only for the decay-in-flight experiments.

^{59}Ge, ^{63}Se, ^{67}Kr. Special calculations have not been done for these nuclei. However, the lifetime systematics for them should be similar to their even neighbors. Based on the separation energy calculations [27,28] (see Table II) we can expect that here the 2*p* branch is likely to be suppressed by weak transitions. The same should also be true for ^{71}Sr if we stick to the same calculations of separation energy: it is clear

that with about 2 MeV of decay energy this nucleus should have too long 2*p* decay lifetime compared to expected weak lifetime.

VI. CONCLUSION

In this paper we have performed systematic studies of the prospective two-proton emitters: ^{45}Fe, ^{48}Ni, ^{54}Zn, ^{58,59}Ge, ^{62,63}Se, and ^{66,67}Kr. Together with the lighter 2*p* emitters (^{12}O, ^{16}Ne, ^{19}Mg, ^{30}Ar, and ^{34}Ca), studied in the previous publications [1–6], this gives a practically complete picture of experimental opportunities to study this interesting decay mode along the proton dripline with $Z<40$.

The largest uncertainty of the predicted 2*p* decay lifetimes is connected with uncertainty of the separation energies of the prospective 2*p* emitters. We have seen that in many cases the precision of the available separation energy predictions is yet insufficient to be practically useful. The next relatively small source of the uncertainty is a structural uncertainty connected with the configuration mixing in the *s-d* shell and especially in the *p-f* shell nuclei. A detailed insight in the properties of the model in that respect is provided by the example of ^{45}Fe. In the framework of our model, if the lifetime is considered to be precisely known, then the structural uncertainty implies 150–250 keV uncertainty in the separation energy at most.

Some aspects of correlations among decay products are discussed. For ^{19}Mg and ^{45}Fe we also make detailed calculations of the possible correlations in the decay and consider their connections with other properties of the systems. We study convergence and stability of the momentum distributions. We also demonstrate that valuable information can be obtained from incomplete information about correlations (projected distributions). The different theoretical models are still distinguishable in such case.

The studies underline the importance of further investigation of ^{45}Fe, including, if possible, studies of correlations among the decay products. The ^{19}Mg and ^{54}Zn seem to be the most "reliable" and promising candidates for pioneering experiments. Possible candidates are also ^{48}Ni (for implantation experiments) and ^{30}Ar, ^{58}Ge, ^{62}Se, ^{66}Kr (for decay-in-flight studies).

ACKNOWLEDGMENTS

We are grateful to I. G. Mukha, who actively collaborated with us on different stages of this work. Valuable discussions with B. Blank, B. A. Brown, G. Giovinazzio, M. Pfützner, and K. Sümmerer are acknowledged. We are grateful to G. Nyman, B. Jonson, and M. Meister for careful reading of the manuscript and useful comments. The authors acknowledge the financial support from the Royal Swedish Academy of Science. L.V.G. acknowledge the hospitality of the Chalmers University of Technology, where part of this work was done. L.V.G. was partly supported by Russian RFBR Grant No. 00-15-96590 and Ministry of Industry and Science Grant No. NS-1885.2003.2.

[1] L. V. Grigorenko, R. C. Johnson, I. G. Mukha, I. J. Thompson, and M. V. Zhukov, Phys. Rev. Lett. **85**, 22 (2000).
[2] L. V. Grigorenko, R. C. Johnson, I. G. Mukha, I. J. Thompson, and M. V. Zhukov, Phys. Rev. C **64**, 054002 (2001).
[3] L. V. Grigorenko, I. G. Mukha, I. J. Thompson, and M. V. Zhukov, Phys. Rev. Lett. **88**, 042502 (2002).
[4] L. V. Grigorenko, R. C. Johnson, I. G. Mukha, I. J. Thompson, and M. V. Zhukov, Eur. Phys. J. A **15**, 125 (2002).
[5] L. V. Grigorenko, I. G. Mukha, and M. V. Zhukov, Nucl. Phys. **A713**, 372 (2003).
[6] L. V. Grigorenko, I. G. Mukha, and M. V. Zhukov, Nucl. Phys. **A714**, 425 (2003).
[7] V. I. Goldansky, Nucl. Phys. **19**, 482 (1960).
[8] J. Jänecke, Nucl. Phys. **61**, 326 (1965).
[9] A. I. Baz', V. I. Goldansky, V. Z. Goldberg, and Ya. B. Zeldovich, *Light and Intermediate Nuclei Near the Border of Nuclear Stability* (Nauka, Moscow, 1972).
[10] B. A. Brown, Phys. Rev. C **43**, R1513 (1991); **44**, 924(E) (1991).
[11] W. Nazarewicz *et al.*, Phys. Rev. C **53**, 740 (1996).
[12] F. C. Barker, Phys. Rev. C **63**, 047303 (2001).
[13] P. J. Woods and C. N. Davids, Annu. Rev. Nucl. Part. Sci. **47**, 541 (1997).
[14] M. Pfützner *et al.*, Eur. Phys. J. A **14**, 279 (2002).
[15] J. Giovinazzo *et al.*, Phys. Rev. Lett. **89**, 102501 (2002).
[16] I. Mukha and G. Schrieder, Nucl. Phys. **A690**, 280c (2001).
[17] M. Meister *et al.*, Nucl. Phys. **A723**, 13 (2003); Phys. Rev. Lett. **91**, 162504 (2003).
[18] A. Brown (private communication).
[19] O. V. Bochkarev *et al.*, Nucl. Phys. **A505**, 215 (1989).
[20] B. A. Brown and F. C. Barker, Phys. Rev. C **67**, 041304(R) (2003).
[21] G. Audi and A. H. Wapstra, Nucl. Phys. **A565**, 1 (1993); **A565**, 66 (1993).
[22] P. Descouvemont, Nucl. Phys. **80**, 99 (1966).
[23] G. Audi and A. H. Wapstra, Nucl. Phys. **A595**, 409 (1995).
[24] B. J. Cole, Phys. Rev. C **56**, 1866 (1997).
[25] W. E. Ormand, Phys. Rev. C **53**, 214 (1996).
[26] B. J. Cole, Phys. Rev. C **54**, 1240 (1996).
[27] W. E. Ormand, Phys. Rev. C **55**, 2407 (1997).
[28] B. A. Brown *et al.*, Phys. Rev. C **65**, 045802 (2002).
[29] R. A. Kryger *et al.*, Phys. Rev. Lett. **74**, 860 (1995).
[30] F. Pougeon (private communication).
[31] B. Blank *et al.*, Phys. Rev. Lett. **84**, 1116 (2000).